

# Machine Learning Exchange-Correlation Potential in Time-Dependent Density Functional Theory

Yasumitsu Suzuki,<sup>1,\*</sup> Ryo Nagai,<sup>2,3</sup> and Jun Haruyama<sup>3</sup>

<sup>1</sup>*Department of Physics, Tokyo University of Science, 1-3 Kagurazaka, Shinjuku-ku, Tokyo 162-8601, Japan*

<sup>2</sup>*Department of Physics, The University of Tokyo, Hongo, Bunkyo-ku, Tokyo 113-0033, Japan*

<sup>3</sup>*Institute for Solid State Physics, The University of Tokyo, Kashiwa, Chiba 277-8581, Japan*

(Dated: November 4, 2022)

We propose a machine learning based approach to develop the exchange-correlation potential of time-dependent density functional theory. The neural-network projection from the time-varying electron densities to the corresponding correlation potentials in the time-dependent Kohn-Sham equation is trained using a few exact datasets for a model system of electron-hydrogen scattering. We demonstrate that this neural-network potential can capture the complex structures in the time-dependent correlation potential during the scattering process and provide correct scattering probabilities, which are not obtained by the standard adiabatic functionals. We also show that it is possible to systematically incorporate the nonadiabatic (or *memory*) effect in the potential with this machine learning technique, which significantly improves the accuracy of the dynamics. The method developed here offers a novel way to improve the exchange-correlation potential of time-dependent density functional theory, which makes the theory a more powerful tool to study various excited state phenomena.

Time-dependent density functional theory (TDDFT) [1–3] is a widely used first-principles approach to study the excited state properties of atoms, molecules and solids. TDDFT enables the first-principles simulation of correlated many-electron dynamics, which is in principle described by the time-dependent Schrödinger equation (TDSE) for the interacting system, by mapping it to the dynamics of the noninteracting [also called Kohn-Sham (KS)] system evolving in a single-particle potential. There have been many successful applications of TDDFT simulation to the interpretation and prediction of various excited state phenomena, e.g., the linear response and spectra of molecules and solids [4–8], and real-time electron dynamics in systems exposed to external fields [9–14] and in various non-equilibrium situations [15–20].

TDDFT is a formally exact theory, i.e., it ensures that the TDSE for the noninteracting (KS) system,

$$i\frac{\partial}{\partial t}\Phi_{\text{KS}}(\underline{\mathbf{r}},t) = \left(\sum_{i=1}^N\left[-\frac{\nabla_i^2}{2} + v_{\text{ext}}(\mathbf{r}_i,t)\right] + v_{\text{H}}[n](\mathbf{r}_i,t) + v_{\text{XC}}[n,\Psi_0,\Phi_0](\mathbf{r}_i,t)\right)\Phi_{\text{KS}}(\underline{\mathbf{r}},t), \quad (1)$$

can, in theory, yield any observables of an  $N$ -electron system exactly and solely from the time-dependent electron density  $n(\mathbf{r},t) = N \int d^{N-1}\mathbf{r}' |\Phi_{\text{KS}}(\underline{\mathbf{r}},t)|^2$ . (Throughout this paper, atomic units are used unless stated otherwise, and  $\underline{\mathbf{r}} \equiv \{\mathbf{r}_1, \mathbf{r}_2, \dots, \mathbf{r}_N\}$ .) Here,  $v_{\text{ext}}(\mathbf{r},t)$  and  $v_{\text{H}}(\mathbf{r},t)$  are the external potential applied to the system and the Hartree potential ( $v_{\text{H}}(\mathbf{r},t) = \int d\mathbf{r}' \frac{n(\mathbf{r}',t)}{|\mathbf{r}-\mathbf{r}'|}$ ), respectively, and  $v_{\text{XC}}(\mathbf{r},t)$  is the time-dependent (TD) exchange-correlation (XC) potential, which incorporates

all many-body effects in the theory. The unique existence of the TDXC potential is proved by the Runge-Gross [1] and van Leeuwen [21] theorems; however, its exact form is unknown. It is known that the exact TDXC potential  $v_{\text{XC}}[n,\Psi_0,\Phi_0](\mathbf{r},t)$  at time  $t$ , in principle, is functionally dependent on the history of the density  $n(\mathbf{r},t' < t)$ , the initial interacting many-body state  $\Psi_0$ , and the choice of the initial KS state  $\Phi_0$ , which indicates its exact form should be extremely complicated.

Therefore, almost all TDDFT applications to date use an adiabatic approximation, which inputs the instantaneous density into one of the existing XC potential functionals in the *ground-state* density functional theory (DFT) [22], and completely neglects both the history and initial-state dependence, i.e., lacks the *memory effect* [2, 23]. It is true that the TDDFT calculation with these adiabatic functionals has achieved significant success in many studies [24–32]. However, it has also been reported that there are many situations where these approximate TDXC potentials fail to even qualitatively reproduce the true dynamics [33–36]. Recent studies on exactly-solvable model systems [37–45] have extensively explored the conditions where the adiabatic functional fails. One important finding is that, when the local acceleration of electron densities occurs, the correlation part ( $v_{\text{C}}$ ) of the exact TDXC potential  $v_{\text{XC}} (= v_{\text{X}} + v_{\text{C}})$ , exhibits complex dynamical structures [37, 43] that arise from the memory effect and play significant roles to provide the correct dynamics. The electron scattering process is a typical situation where these complex structures in the TD correlation (TDC) potential appear, and it was revealed that the standard adiabatic functionals lack these structures [43, 44].

In this study, we propose a novel approach to improve the XC potential of TDDFT using a machine learning technique. Development of the XC functional in *DFT* by a machine learning based approach has been actively

\* yasumitsu.suzuki@rs.tus.ac.jp

conducted recently [46–51], which demonstrates it is a promising direction to improve the DFT. In particular, neural-network (NN) projection from the electron density to the ground-state XC potential was developed in a recent study [49], and it was demonstrated that the KS equation equipped with this NN functional provides accurate ground-state density and total energy for a one-dimensional two-electron model system, and has a remarkable transferability. In TDDFT, the TDC potential functional can also be regarded as a projection  $n \rightarrow v_{XC}$ , but here  $n$  is the history of the density ( $n(\mathbf{r}, t' < t)$ ). Thus, the projection should be more complicated than that in DFT, which means that there is more expectation on a machine learning based approach to find such a complicated projection.

Here we construct the NN projection from the TD density  $n(\mathbf{r}, t)$  to the TDC potential  $v_C(\mathbf{r}, t)$  for a model system of electron-hydrogen (e-H) scattering [43, 44], as one example where the existing approximate functionals fail to reproduce the complex structures in  $v_C(\mathbf{r}, t)$ . We demonstrate that this NN TDC potential  $v_{TDC}^{NN}$  captures the complex structures that appeared in the exact potential very well, and provide significantly improved time-resolved scattering dynamics compared to those obtained by the standard approximate functionals.

The e-H scattering model system studied in this work is the same as that used in the previous studies [43, 44]. It is a one-dimensional two-electron system with the Hamiltonian:  $\hat{H}(x_1, x_2) = \sum_{i=1,2} \left( -\frac{1}{2} \frac{\partial^2}{\partial x_i^2} + v_{\text{ext}}(x_i) \right) + W_{ee}(x_1, x_2)$ , where  $W_{ee}(x_1, x_2) = \frac{1}{\sqrt{(x_1 - x_2)^2 + 1}}$  is the soft-Coulomb interaction [52–58] and the external potential  $v_{\text{ext}}(x) = -\frac{1}{\sqrt{(x+10)^2 + 1}}$  is the soft-Coulomb model of a H atom located at  $x = -10.0$  a.u. The spatial part of the initial interacting wavefunction is  $\Psi_0(x_1, x_2) = \frac{1}{\sqrt{2}} (\phi_H(x_1)\phi_{WP}(x_2) + \phi_{WP}(x_1)\phi_H(x_2))$ , where a singlet state is chosen for the spin part.  $\phi_H(x)$  is the ground-state of one electron alone in the external potential  $v_{\text{ext}}(x)$  and  $\phi_{WP}(x) = (2\alpha/\pi)^{\frac{1}{4}} e^{[-\alpha(x-x_0)^2 + ip(x-x_0)]}$  is an incident Gaussian wavepacket ( $\alpha = 0.1$ ), which represent an electron initially localized at  $x_0 = 10.0$  a.u. approaching the H atom with a certain momentum  $p$ . For this system, the full TDSE  $i\partial_t\Psi(x_1, x_2, t) = \hat{H}(x_1, x_2)\Psi(x_1, x_2, t)$  can be numerically solved exactly, and the resulting TD density (for the case of incident momentum  $p = -1.5$  a.u. for our first example), which were already reported in Ref. [43], are plotted as the red lines in the upper panel for different time slices in Fig. 1. As reported previously [43], for this case of  $p = -1.5$  a.u., the scattering is inelastic, and some part of the wavepacket is reflected back after the collision at around 0.24 fs.

For this two-electron dynamics, the exact TDC potential can be numerically obtained for any choice of the valid initial KS state that satisfies the van Leeuwen theorem [39, 42]. Here, we focus on one natural choice for the initial KS state, i.e., the Slater determinant [42, 43]:

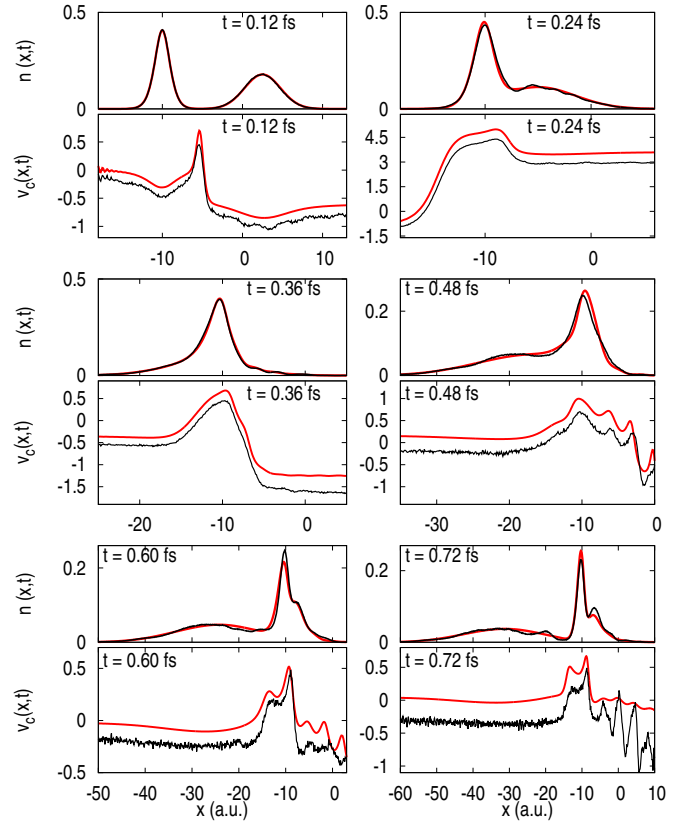


FIG. 1. Snapshots of the trained NN TDC potential  $v_{TDC}^{NN}$  for the initial KS state  $\Phi_0^{(1)}$  in the e-H scattering model system (black line in the lower panel for each time slice) and the corresponding TD electron densities (black line in the upper panel) obtained by propagating the TDKS equation equipped with  $v_{TDC}^{NN}$ . Exact electron density (red line in the upper panel) and the exact TDC potential  $v_{TDC}^{\text{exact}}$  (red line in the lower panel) are also plotted for each time slice.

$\Phi_0^{(1)}(x_1, x_2) = \phi_0(x_1)\phi_0(x_2)$  with one doubly-occupied spatial orbital  $\phi_0(x) = \sqrt{\frac{n_0(x)}{2}} \exp \left[ i \int^x \frac{j_0(x')}{n_0(x')} dx' \right]$ , where  $n_0$  and  $j_0$  are respectively the initial density and current density of the interacting system. For this initial KS state  $\Phi_0^{(1)}$ , the exact  $v_X(x, t)$  and  $v_C(x, t)$  can be numerically calculated [2, 37, 59, 60] using the exact TD density  $n(x, t)$  and current density  $j(x, t)$  obtained from the solution of the TDSE. The numerically obtained  $v_C^{\text{exact}}(x, t)$  (shown as the red lines in the lower panels of Fig. 1) exhibit complex peak- and valley-like structures that are crucial for scattering [43].

In this study, we aim to make the NN learn this exact TD correlation potential  $v_C^{\text{exact}}(x, t)$  because the exact functional form of  $v_X^{\text{exact}}(x, t)$  ( $= -\frac{1}{2} \int dx' W_{ee}(x', x) n(x', t)$ ) is already known for the system under focus [2, 37]. The structure of the NN TDC potential  $v_{TDC}^{NN}$  constructed here is expressed as:

$$\mathbf{v}_{TDC}^{NN} = \dots f[W^{(2)} f[W^{(1)} \mathbf{n} + \mathbf{b}^{(1)}] + \mathbf{b}^{(2)}] \dots, \quad (2)$$

where  $\mathbf{v}_{TDC}^{NN}$  and  $\mathbf{n}$  are the vectorized representations of

$v_{\text{TDC}}^{\text{NN}}$  and  $n$  ( $f$  is a non-linear activation function (ReLU function [61] here), and  $W^{(l)}$  ( $l = 1, 2, \dots$ ) and  $\mathbf{b}^{(l)}$  are the weight matrices and bias vectors, of which the components are optimized to minimize the training error). As with the study on the NN XC potential in DFT [49], the form of Eq. (2) is, in principle, sufficiently flexible to be a numerically exact TDC potential. The input vector  $\mathbf{n}$  should ideally represent the entire history of the density ( $n(\mathbf{r}, t' < t)$ ); however, in the first example, the instantaneous density  $n(\mathbf{r}, t)$  is used as  $\mathbf{n}$ .

The training procedure of the first example is as follows. First, the learning data set ( $\mathbf{n}^{(i)}(t_j)$ ,  $\mathbf{v}_{\text{TDC}}^{(i)}(t_j)$ ) is generated from the numerical calculation of  $n(x, t)$  and  $v_{\text{C}}^{\text{exact}}(x, t)$ . Here,  $i$  is the index that corresponds to the different scattering dynamics calculation with a different initial incident momentum,  $p$ . In this study, five different initial momenta;  $p = -1.0, -1.2, -1.4, -1.6, -1.8$  were employed to generate the training data set (thus  $i = 1, \dots, 5$ ). For each calculation with different  $p$ , the TDSE was numerically propagated up to  $t = 0.72$  fs, which corresponds to 300 time steps, and thus  $j = 1, \dots, 300$ . Therefore, the  $5 \times 300 = 1500$  data set of ( $\mathbf{n}^{(i)}(t_j)$ ,  $\mathbf{v}_{\text{TDC}}^{(i)}(t_j)$ ) was generated.  $\mathbf{n}^{(i)}(t_j)$  and  $\mathbf{v}_{\text{TDC}}^{(i)}(t_j)$  are the vectors obtained by the real-space discretization of  $n^{(i)}(x, t_j)$  and  $v_{\text{TDC}}^{(i)}(x, t_j)$ , respectively, onto common  $N_r = 1200$  uniform mesh points, i.e.,  $\mathbf{n}^{(i)}(t_j) = \{n^{(i)}(x_1, t_j), n^{(i)}(x_2, t_j), \dots, n^{(i)}(x_{N_r}, t_j)\}$  and  $\mathbf{v}_{\text{TDC}}^{(i)}(t_j) = \{v_{\text{TDC}}^{(i)}(x_1, t_j), v_{\text{TDC}}^{(i)}(x_2, t_j), \dots, v_{\text{TDC}}^{(i)}(x_{N_r}, t_j)\}$ .

The parameters of the NN (Eq. (2)) are then optimized with the generated data set using a similar method to that reported in Ref. [49]: The fully connected NN with two hidden layers with 1200 nodes are used, and the root mean squared error between  $\mathbf{v}_{\text{TDC}}^{(i)}(t_j)$  and those calculated from  $\mathbf{n}^{(i)}(t_j)$  by the NN is minimized with the adaptive moment estimation method (Adam) [62] algorithm implemented in the *Chainer* package [63]. The initial estimate of the weight parameters is randomly generated and the optimization is stopped after 20000 epochs. Other details of the optimization are the same as those used in Ref. [49]. This optimization procedure is sufficient to provide a NN that gives excellent results, as detailed later.

Finally, the trained NN TDC potential  $v_{\text{TDC}}^{\text{NN}}$  is implemented in the time-dependent Kohn-Sham (TDKS) equation (Eq. (1) for the initial KS state  $\Phi_0^{(1)}$  with an initial incident momentum  $p = -1.5$ , which is out of the  $p$  used for the training, i.e., the test of the present NN is demonstrated by numerically integrating the TDKS equation for  $\Phi_0^{(1)}$ :

$$i \frac{\partial}{\partial t} \phi(x, t) = \left[ -\frac{\nabla^2}{2} + v_{\text{ext}}(x, t) + v_{\text{H}}[n](x, t) + v_{\text{X}}[n](x, t) + v_{\text{TDC}}^{\text{NN}}(x, t) \right] \phi(x, t), \quad (3)$$

over time, where  $n(x, t) = 2|\phi(x, t)|^2$  is calculated and the TDC potential is obtained from the NN  $v_{\text{TDC}}^{\text{NN}}$  on-

the-fly at each time step for the initial condition out of the training data set.

The resultant  $n(x, t)$  and  $v_{\text{TDC}}^{\text{NN}}(x, t)$  are plotted as black lines in the upper and lower panels of Fig. 1. It is evident that  $v_{\text{TDC}}^{\text{NN}}$  captures the complex structures of the exact TDC potential, and the density dynamics reproduce the certain amount of reflection probability. Therefore, the machine learning based approach is confirmed as effective for the numerical implementation of  $v_{\text{TDC}}$ , at least for this first example. From Fig. 1,  $v_{\text{TDC}}^{\text{NN}}$  gradually exhibits spatially oscillating structures as times passes, which is due to the accumulation of small errors in the TD density, an intrinsic problem of the TD calculation that does not exist in the case of the NN potential for DFT. Nevertheless, the TD densities obtained from  $v_{\text{TDC}}^{\text{NN}}$  show rather smooth structures during the entire simulation time (up to  $t = 0.72$  fs). This is achieved by the effect of the kinetic energy operator in Eq. (3) as a regulator of the artificial oscillation, as with that for the DFT case [49].

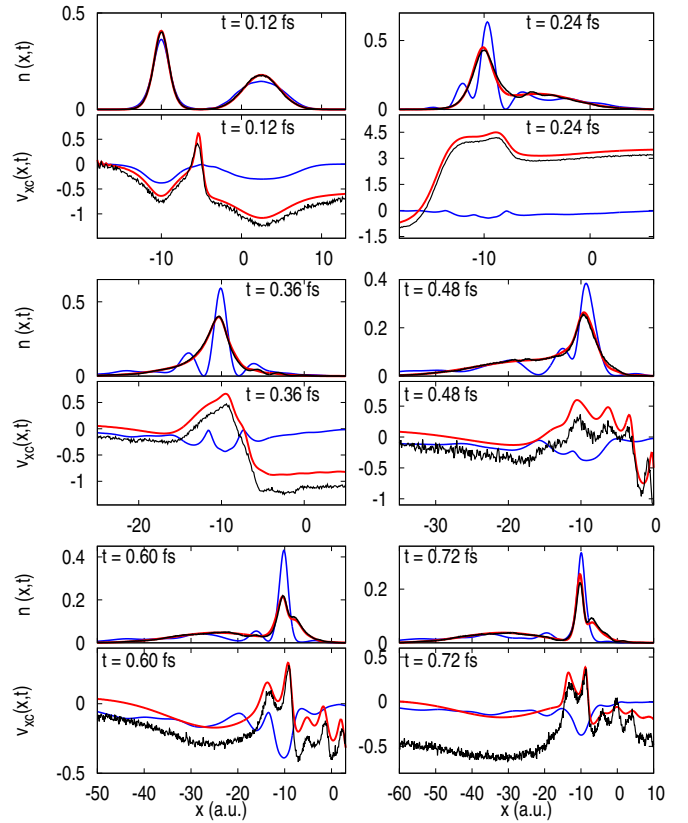


FIG. 2. Snapshots of the NN TDXC potential with the memory effect  $v_{\text{TDC}}^{\text{NNmemory}} = v_{\text{X}} + v_{\text{TDC}}^{\text{NNmemory}}$  for the same system shown in Fig. 1 (black line in the lower panel for each time slice) and the corresponding TD electron densities (black line in the upper panel). Exact (red lines) and ALDA (blue lines) results are also plotted for each time slice.

Now we consider a strategy for improvement of  $v_{\text{TDC}}^{\text{NN}}$ . Our first attempt to develop  $v_{\text{TDC}}^{\text{NN}}$  does not take account of the memory effect of  $n(\mathbf{r}, t' < t)$  explicitly, i.e., the

training data set was the combination of the instantaneous density  $n(x, t)$  and  $v_{\text{TDC}}^{\text{exact}}(x, t)$ . Here we present how to incorporate the memory effect into  $v_{\text{TDC}}^{\text{NN}}$ . We assume that the density distribution immediately before  $t$  has the most effect on  $v_{\text{TDC}}$  at  $t$ . Based on this hypothesis, we propose the following expression for the input vector  $\mathbf{n}$  for the NN (Eq. (2)), so that it takes account of the memory effect:

$$\begin{aligned} \mathbf{n}^{(i)}(t_j, t_j - \Delta t, \dots, t_j - m\Delta t) \\ = \{\mathbf{n}^{(i)}(t_j), \mathbf{n}^{(i)}(t_j - \Delta t), \dots, \mathbf{n}^{(i)}(t_j - m\Delta t)\}, \end{aligned} \quad (4)$$

where  $\Delta t$  is the time step used for the numerical propagation and  $m$  is an integer parameter that controls how previous densities are taken into account.  $\mathbf{n}^{(i)}(t_j, t_j - \Delta t, \dots, t_j - m\Delta t)$  is related to  $\mathbf{v}_{\text{TDC}}^{(i)}(t_j)$  as one learning data set, i.e., the NN TDC potential trained with the memory effect,  $v_{\text{TDC}}^{\text{NNmemory}}$ , maps  $\mathbf{n}(t_j, t_j - \Delta t, \dots, t_j - m\Delta t)$  to  $\mathbf{v}_{\text{TDC}}(t_j)$  at each time  $t_j$ .

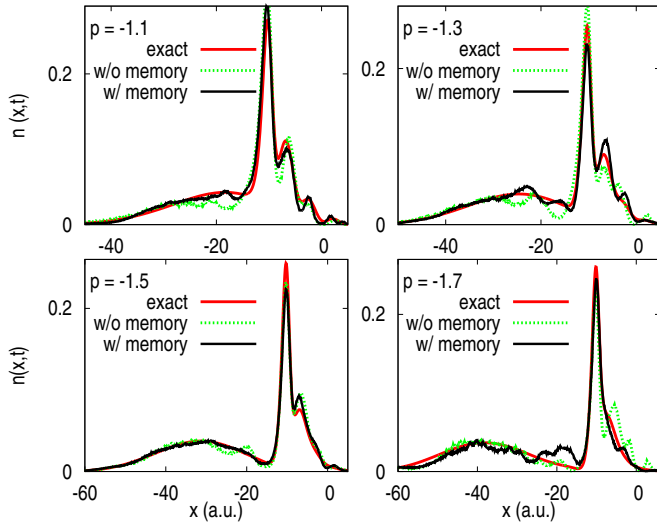


FIG. 3. Snapshots of the electron density at  $t = 0.72$  fs obtained from different calculations: the exact TDSE calculation (red solid line), the TDKS equation equipped with the NN TDC potential without the memory effect (green dotted line), and with the memory effect (black solid line). The four panels correspond to the different initial incident momentum  $p = -1.1$  (upper left),  $-1.3$  (upper right),  $-1.5$  (lower left), and  $-1.7$  (lower right).

We investigate the effectiveness of this method with  $m = 1$  as a first attempt.  $v_{\text{TDC}}^{\text{NNmemory}}$  is trained using a similar procedure to that without the memory effect (The only difference is that the number of input nodes is now double, i.e.,  $1200 \times 2 = 2400$ . The number of hidden layer nodes is retained as 1200). Figure 2 shows snapshots of the NN TDC potential with memory, i.e.,  $v_{\text{TDC}}^{\text{NNmemory}} = v_X + v_{\text{TDC}}^{\text{NNmemory}}$  (black solid line in the lower panels) and the TD density (black solid lines in the upper panels) obtained through the solution of the TDKS equation with this NN potential. A comparison of

these results with the exact results (red lines) reveals remarkable agreement between them, and the results obtained from the NN with memory shows better agreement than those obtained without memory (Fig. (1)); this is presented more clearly in Figs. 3 and 4 discussed later. We note that the exact TDC potential (red line in the lower panels of Fig. (2)) and the exact TDC potential (red line in the lower panels of Fig. (1)) have almost the same structure, which indicates that the contribution of the TDC potential is small. It was previously reported that the dynamics calculated with only the exact TDC potential functional fail to reproduce the correct scattering [43, 44]; therefore, it is essential to capture the features of the exact TDC potential correctly. In Fig. 2, the results obtained using the adiabatic local density approximation (ALDA) [64–66] to both the exchange and correlation potentials are also plotted as blue lines (same as those reported in Ref. [43]). The ALDA XC potential, and other standard XC functionals (reported in Ref. [43, 44]), lack the important memory effect, and their structures are significantly different from the exact structure, which leads to a failure to yield the correct scattering. The NN TDC potential presented here, both with and without the memory effect, provides significantly better results than those from the standard functionals.

To show the impact of incorporating the memory effect, we plot a comparison of the electron density at  $t = 0.72$  fs obtained from the different calculations in Fig. 3; the exact TDSE calculation (red solid line), the TDKS equation equipped with the NN TDC potential without the memory effect (green dotted line) and with the memory effect (black solid line) for the four different dynamics that start with different initial incident momenta;  $p = -1.1, -1.3, -1.5$ , and  $-1.7$  (indicated inside each panel). None of these  $p$  values are referenced in the training of the NN; therefore, the out-of-training transferability of the NN can also be checked from Fig. 3. These results indicate that the NN potential, both with memory and without memory, reproduces the exact density for all  $p$  cases, and thus demonstrates its out-of-training transferability. Furthermore, in all  $p$  cases, the density from the NN with memory has better agreement with the exact density than that from the NN without memory (this is also confirmed by Fig. 4; see below), which indicates a part of the memory effect is taken into account by the addition of  $n$  from the previous time step into the input to the NN.

To clearly reveal the superiority of the NN with memory over that without memory, the time evolution of the number of electrons reflected (transmitted),  $N_R$  ( $N_T$ ), which is defined as the integral of the density over the region  $x > -5.0$  a.u. ( $x < -15.0$  a.u.), is plotted for all  $p$  in Fig. 4 (red solid line: the exact, green dotted line: the NN TDC without memory, black solid line: the NN TDC with memory, and blue solid line: ALDA). This figure confirms the present findings: the NN TDC with memory gives better results (almost of the same as the exact



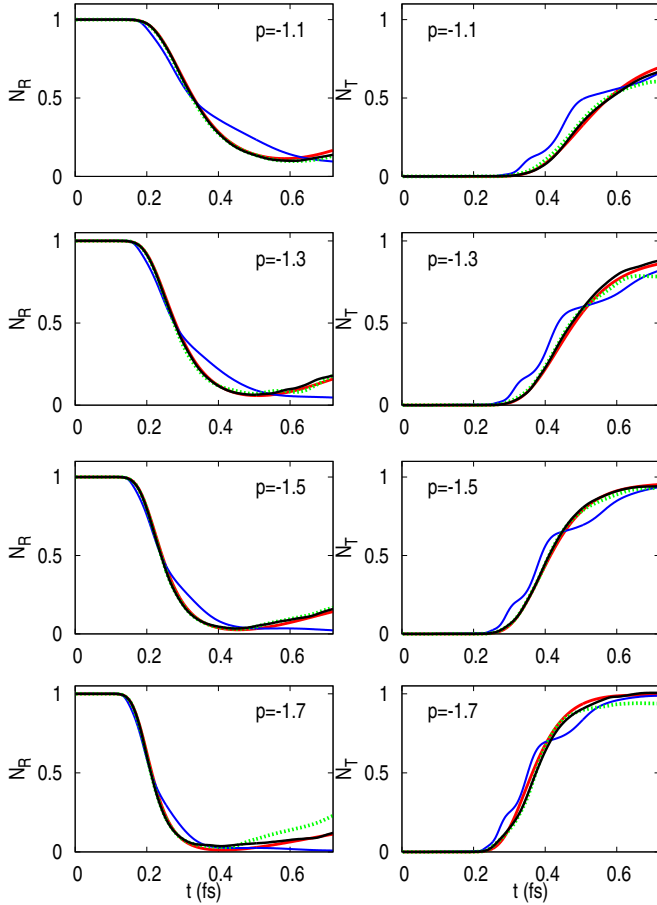


FIG. 4. Number of electrons in the reflection region  $N_R$  (left panel) and transmission region  $N_T$  (right panel) for the exact (red solid line), NN TDC potential without the memory effect (green dotted line) and with the memory effect (black solid line), and ALDA (blue solid line) for the four different initial incident momenta;  $p = -1.1, -1.3, -1.5$ , and  $-1.7$  (indicated inside each panel).

result) than the NN TDC without memory for all  $p$  cases. Therefore, the validity of the proposed strategy to incorporate the memory effect by modification of the input density vector to Eq. (4) is demonstrated. On the other hand, the ALDA gives poor results and is particularly problematic in the reproduction of the correct reflection.

The two types of NNs developed here are already superior to the ALDA and other standard XC functionals, at least for the model scattering problem investigated here. This indicates that these NN TDC potential successfully captures not only the space nonlocality [22, 67], which is important to match the exact TDX potential, but also the time nonlocality (memory effect) that was reported to be crucial for the time-resolved scattering dynamics [43, 44]. With regard to the reason why the first NN that does not explicitly take account of the memory effect (i.e., the input to the NN is only the instantaneous density) gives better results than the standard adiabatic functionals such as ALDA, we attribute

this to all the dynamics included in the training data set having started from similar initial states, which implicitly imposes an initial condition on the NN, so that the first NN could effectively take account of a part of the memory effect.

With respect to the transferability of the NN, the accuracy of the dynamics obtained from the NN worsened when it is applied to the dynamics of  $p$  in the region of  $p < -1.8$  or  $p > -1.0$  (Data not shown here.). This indicates that expansion of the region where the NN TDC potential can be applied requires more characteristic dynamics to be included in the training data set. This situation is similar to that of the NN for the DFT, where the possible characteristic states need to be included in the training data set to make the NN have a wider transferability [49].

Further systematic improvement of the NN is expected by an increase in the parameter  $m$ . Different strategies to incorporate the memory effect in the NN can also be considered, such as application of the several established methods that take account of the space nonlocality [22, 51] to the time regime, and also by explicitly adding the initial KS state to the training data set. The use of the recurrent neural network (RNN) [68] and long short term memory (LSTM) [69] is also expected to show promise.

In summary, we have presented one example that indicates a novel approach by the application of the machine learning technique to develop the XC potential of TDDFT is effective. We have demonstrated that the NN TDC potential trained with a few numerically exact data sets reproduces the correct 1-dimensional two-electron scattering dynamics that are not included in the training data, which demonstrates its transferability. Furthermore, we have also shown that it is possible to systematically incorporate the memory effect in this NN TDC potential, and the lowest order memory (including the density just before  $t$  in the input to the NN) is shown to improve the result.

Our results indicate that once a few numerically exact (or sufficiently accurate) data of the many-body dynamics of interest are available, then it is possible to train the NN TDC (or TDXC) potential so that it can be used to simulate at least similar dynamics to those used in the training. For example, the TDSE of an (three-dimensional) atom in a laser field can be numerically solved by means of the time-dependent variational principle method [70], and the resulting data can be used to train the NN TDXC potential, which can then be applied to the TDDFT calculation of actual molecules. It will also be possible to apply the machine learning approach to develop the XC kernel in linear-response TDDFT [4–7] using the many-body perturbation calculation results as training data. With these studies, TDDFT will become a more powerful tool for the study of various excited state phenomena.

## ACKNOWLEDGMENTS

YS is supported by JSPS KAKENHI Grant No. JP19K03675. Part of the computations were performed

on the supercomputers at the Institute for Solid State Physics, The University of Tokyo.

- 
- [1] E. Runge and E. K. U. Gross, Phys. Rev. Lett. **52**, 997 (1984).
  - [2] C. A. Ullrich, *Time-Dependent Density-Functional Theory: Concepts and Applications* (Oxford University Press, 2012).
  - [3] N. T. Maitra, J. Chem. Phys. **144**, 220901 (2016).
  - [4] S. Botti, A. Schindlmayr, R. D. Sole, and L. Reining, Rep. Prog. Phys. **70**, 357 (2007).
  - [5] C. Adamo and D. Jacquemin, Chem. Soc. Rev. **42**, 845 (2013).
  - [6] M. E. Casida and M. Huix-Rotllant, Annu. Rev. Phys. Chem. **63**, 287 (2012).
  - [7] Y.-M. Byun and C. A. Ullrich, Phys. Rev. B **95**, 205136 (2017).
  - [8] Y. Suzuki and K. Watanabe, Phys. Chem. Chem. Phys. **22**, 2908 (2020).
  - [9] P. Wopperer, P. Dinh, P.-G. Reinhard, and E. Suraud, Phys. Rep. **562**, 1 (2015).
  - [10] J. Chen, U. Bovensiepen, A. Eschenlohr, T. Müller, P. Elliott, E. K. U. Gross, J. K. Dewhurst, and S. Sharma, Phys. Rev. Lett. **122**, 067202 (2019).
  - [11] A. Yamada and K. Yabana, Phys. Rev. B **99**, 245103 (2019).
  - [12] H. Hübener, U. De Giovannini, and A. Rubio, Nano Lett. **18**, 1535 (2018).
  - [13] M. Dauth, M. Graus, I. Schelter, M. Wießner, A. Schöll, F. Reinert, and S. Kümmel, Phys. Rev. Lett. **117**, 183001 (2016).
  - [14] A. Umerbekova, S.-F. Zhang, S. Kumar P., and M. Pavanello, Eur. Phys. J. B **91**, 214 (2018).
  - [15] S. Kurth, G. Stefanucci, E. Khosravi, C. Verdozzi, and E. K. U. Gross, Phys. Rev. Lett. **104**, 236801 (2010).
  - [16] Y. Ueda, Y. Suzuki, and K. Watanabe, Phys. Rev. B **97**, 075406 (2018).
  - [17] B. F. E. Curchod, U. Rothlisberger, and I. Tavernelli, ChemPhysChem **14**, 1314 (2013).
  - [18] S. Kurth and G. Stefanucci, J. Phys.: Condens. Matter **29**, 413002 (2017).
  - [19] C. Pellegrini, J. Flick, I. V. Tokatly, H. Appel, and A. Rubio, Phys. Rev. Lett. **115**, 093001 (2015).
  - [20] Y. Suzuki, S. Hagiwara, and K. Watanabe, Phys. Rev. Lett. **121**, 133001 (2018).
  - [21] R. van Leeuwen, Phys. Rev. Lett. **82**, 3863 (1999).
  - [22] W. Koch and M. C. Holthausen, *A Chemist's Guide to Density Functional Theory* (Wiley-VCH, 2001).
  - [23] N. T. Maitra, K. Burke, and C. Woodward, Phys. Rev. Lett. **89**, 023002 (2002).
  - [24] C. A. Rozzi, S. M. Falke, N. Spallanzani, A. Rubio, E. Molinari, D. Brida, M. Maiuri, G. Cerullo, H. Schramm, J. Christoffers, and C. Lienau, Nat. Commun. **4**, 1602 (2013).
  - [25] E. Penka Fowe and A. D. Bandrauk, Phys. Rev. A **84**, 035402 (2011).
  - [26] K. Yabana, T. Sugiyama, Y. Shinohara, T. Otobe, and G. F. Bertsch, Phys. Rev. B **85**, 045134 (2012).
  - [27] A. Castro, J. Werschnik, and E. K. U. Gross, Phys. Rev. Lett. **109**, 153603 (2012).
  - [28] Y. Miyamoto, H. Zhang, T. Miyazaki, and A. Rubio, Phys. Rev. Lett. **114**, 116102 (2015).
  - [29] Z. Wang, S.-S. Li, and L.-W. Wang, Phys. Rev. Lett. **114**, 063004 (2015).
  - [30] P. Elliott, K. Krieger, J. K. Dewhurst, S. Sharma, and E. K. U. Gross, New J. Phys. **18**, 013014 (2016).
  - [31] A. Schleife, Y. Kanai, and A. A. Correa, Phys. Rev. B **91**, 014306 (2015).
  - [32] E. E. Quashie, B. C. Saha, X. Andrade, and A. A. Correa, Phys. Rev. A **95**, 042517 (2017).
  - [33] S. Raghunathan and M. Nest, J. Chem. Theory Comput. **8**, 806 (2012).
  - [34] B. F. Habenicht, N. P. Tani, M. R. Provorse, and C. M. Isborn, J. Chem. Phys. **141**, 184112 (2014).
  - [35] M. R. Provorse and C. M. Isborn, Int. J. Quantum. Chem. **116**, 739 (2016).
  - [36] H. O. Wijewardane and C. A. Ullrich, Phys. Rev. Lett. **95**, 086401 (2005).
  - [37] P. Elliott, J. I. Fuks, A. Rubio, and N. T. Maitra, Phys. Rev. Lett. **109**, 266404 (2012).
  - [38] K. Luo, J. I. Fuks, E. D. Sandoval, P. Elliott, and N. T. Maitra, J. Chem. Phys. **140**, 18A515 (2014).
  - [39] J. I. Fuks, S. E. B. Nielsen, M. Ruggenthaler, and N. T. Maitra, Phys. Chem. Chem. Phys. **18**, 20976 (2016).
  - [40] M. Thiele, E. K. U. Gross, and S. Kümmel, Phys. Rev. Lett. **100**, 153004 (2008).
  - [41] J. D. Ramsden and R. W. Godby, Phys. Rev. Lett. **109**, 036402 (2012).
  - [42] P. Elliott and N. T. Maitra, Phys. Rev. A **85**, 052510 (2012).
  - [43] Y. Suzuki, L. Lacombe, K. Watanabe, and N. T. Maitra, Phys. Rev. Lett. **119**, 263401 (2017).
  - [44] L. Lacombe, Y. Suzuki, K. Watanabe, and N. T. Maitra, Eur. Phys. J. B **91**, 96 (2018).
  - [45] N. Dittmann, J. Splettstoesser, and N. Helbig, Phys. Rev. Lett. **120**, 157701 (2018).
  - [46] J. C. Snyder, M. Rupp, K. Hansen, K.-R. Müller, and K. Burke, Phys. Rev. Lett. **108**, 253002 (2012).
  - [47] F. Brockherde, L. Vogt, L. Li, M. E. Tuckerman, K. Burke, and K.-R. Müller, Nat. Commun. **8**, 872 (2017).
  - [48] L. Li, T. E. Baker, S. R. White, and K. Burke, Phys. Rev. B **94**, 245129 (2016).
  - [49] R. Nagai, R. Akashi, S. Sasaki, and S. Tsuneyuki, J. Chem. Phys. **148**, 241737 (2018).
  - [50] J. Schmidt, C. L. Benavides-Riveros, and M. A. L. Marques, J. Phys. Chem. Lett. **10**, 6425 (2019).
  - [51] R. Nagai, R. Akashi, and O. Sugino, arXiv:1903.00238 (2019).
  - [52] J. Javanainen, J. H. Eberly, and Q. Su, Phys. Rev. A **38**, 3430 (1988).
  - [53] D. M. Villeneuve, M. Y. Ivanov, and P. B. Corkum, Phys. Rev. A **54**, 736 (1996).
  - [54] A. D. Bandrauk and N. H. Shon, Phys. Rev. A **66**, 031401(R) (2002).
  - [55] M. Lein, E. K. U. Gross, and V. Engel, Phys. Rev. Lett. **85**, 4707 (2000).

- [56] M. Lein and S. Kümmel, Phys. Rev. Lett. **94**, 143003 (2005).
- [57] D. G. Tempel, T. J. Martínez, and N. T. Maitra, J. Chem. Theory Comput. **5**, 770 (2009).
- [58] L. O. Wagner, E. M. Stoudenmire, K. Burke, and S. R. White, Phys. Chem. Chem. Phys. **14**, 8581 (2012).
- [59] M. Ruggenthaler, M. Penz, and R. van Leeuwen, J. Phys.: Condens. Matter **27**, 203202 (2015).
- [60] S. E. B. Nielsen, M. Ruggenthaler, and R. van Leeuwen, Europhys. Lett. **101**, 33001 (2013).
- [61] X. Glorot, A. Bordes, and Y. Bengio, Proceedings of the Fourteenth International Conference on Artificial Intelligence and Statistics (AISTATS) **15**, 315 (2011).
- [62] D. P. Kingma and J. L. Ba, Proceedings of the 3rd International Conference on Learning Representations (ICLR 2015) (2015).
- [63] *Chainer* (accessed 2019), <https://chainer.org>.
- [64] M. T. Entwistle, M. J. P. Hodgson, J. Wetherell, B. Longstaff, J. D. Ramsden, and R. W. Godby, Phys. Rev. B **94**, 205134 (2016).
- [65] M. Casula, S. Sorella, and G. Senatore, Phys. Rev. B **74**, 245427 (2006).
- [66] N. Helbig, J. I. Fuks, M. Casula, M. J. Verstraete, M. A. L. Marques, I. V. Tokatly, and A. Rubio, Phys. Rev. A **83**, 032503 (2011).
- [67] J. P. Perdew, V. N. Staroverov, J. Tao, and G. E. Scuseria, Phys. Rev. A **78**, 052513 (2008).
- [68] J. J. Hopfield, Proc. Natl. Acad. Sci. USA **79**, 2554 (1982).
- [69] S. Hochreiter and J. Schmidhuber, Neural Comput. **9**, 1735 (1997).
- [70] K. Rowan, L. Schatzki, T. Zaklaman, Y. Suzuki, K. Watanabe, and K. Varga, arXiv:1912.01125 (2019).